AIAA-2003-0753
Transonic Reynolds Number and Leading-Edge Bluntness Effects on a 65^{o} Delta Wing

J. M. Luckring
NASA Langley Research Center
Hampton, Virginia

41st AIAA Aerospace Sciences Meeting & Exhibit
6-9 January 2003
Reno, Nevada

Reynolds Number and Leading-Edge Bluntness Effects on a 65° Delta Wing at Transonic Speeds

J. M. Luckring*
Aerodynamics, Aerothermodynamics, and Acoustics Competency
NASA Langley Research Center
Hampton, Virginia

ABSTRACT

A 65° delta wing has been tested in the National Transonic Facility (NTF) at mean aerodynamic chord Reynolds numbers from 6 million to 120 million at subsonic and transonic speeds. The configuration incorporated a systematic variation of the leading edge bluntness. The analysis for this paper is focused on the Reynolds number and bluntness effects at transonic speeds (M = 0.85) from this data set. The results show significant effects of both these parameters on the onset and progression of leading-edge vortex separation.

NOMENCLATURE

AR	wing aspect ratio, 1.8652
b_{le}	leading-edge bluntness, r_{le}/c_{bar}
b/2	wing semispan, 1.0 ft.
C_p	pressure coefficient
$C_{p,le}$	leading-edge pressure coefficient
$C_{p,v}$	vacuum pressure coefficient
C_p*	sonic pressure coefficient
c	wing chord
c_{bar}	wing mean aerodynamic chord, 1.4297 ft.
c_r	wing root chord, 2.1445 ft.
c_t	wing tip chord, 0 ft.
d	sting diameter, 0.275 ft.
d/b	nondimensional sting diameter, 0.1375
M	Mach number
Rn	Reynolds number, based on c_{bar}
r_{le}	streamwise leading-edge radius
S	wing reference-area, 2.1445 ft^2
t	wing thickness, 0.875 in.
t/c_{bar}	nondimensional wing thickness, 0.051
w_{ts}	NTF test section width, 8.2 ft.
x,y,z	Body-axis Cartesian coordinates
x_m,z_m	match coordinates, leading-edge contour
α	angle of attack
η	percent semispan location, 2y/b
Λ_{le}	wing leading-edge sweep
λ	wing taper ratio, c_t/c_r, 0.

INTRODUCTION

Separation-induced vortex flows have been a topic of research for many decades. At one extreme, these flows have been studied with very simple geometries such as a delta wing. At the other extreme, these flows have been exploited or tolerated with complex full aircraft configurations, such as either the F-16 or the F-18. High-speed and high-performance requirements for maneuvering aircraft often result in wing geometries conducive to this flow. Although high angle-of-attack maneuvering typically occurs at subsonic conditions, the moderate angles of attack associated with transonic maneuver can still result in conditions conducive to the onset and initial progression of flow separation.

Early research for these vortex flows was performed primarily at low speeds and focused on wings with sharp leading edges[1-7] where the primary vortex separation is fixed by this geometric feature. Practical wing designs incorporate blunt leading edges, and this bluntness greatly complicates the aerodynamics of leading-edge vortex flows. Reynolds number and angle of attack sensitivities arise that lead to separation onset and progression effects of the leading edge vortex flow. These effects are absent for wings with sharp leading edges.

Reynolds number effects can exhibit subtle configuration sensitivities and this is especially so for flows involving the onset and progression of separation. Some examples are provided in the references that address these issues for transports[8-10] and fighters.[10-12] With complex configurations it can be difficult to isolate and understand the Reynolds number complexities associated with viscous/inviscid or viscous/viscous flow physics interactions. As such, studies with simpler geometries[13,14] that retain relevant flow physics can provide a useful step toward improved full-scale vehicle prediction capability.

* Senior Research Engineer, Configuration Aerodynamics Branch, Associate Fellow, AIAA

The present investigation is directed at quantifying the effects of leading-edge bluntness and Reynolds number on the onset and progression of leading edge separation for a 65° delta wing at transonic speeds. Selected results are presented from an extensive NTF test.[15-18] The data selected for this analysis were obtained at a free-stream Mach number of 0.85 and at Reynolds numbers of 6 million and 60 million based on the wing mean aerodynamic chord. These Reynolds numbers are representative of conventional ground-based wind tunnel and full-scale flight values, respectively. The Reynolds number analysis presented in this paper will be focused on contrasting data from these two conditions. Limited compressibility effects will also be addressed by contrasting data between freestream Mach numbers of 0.4 and 0.85. A brief description of the experimental program follows. Additional details have recently been summarized.[19]

EXPERIMENTAL PROGRAM

The delta wing program was one of the original fundamental tests planned for the NTF. It was envisioned that these data would serve as a good initial assessment of leading-edge bluntness and Reynolds number effects on vortex flow aerodynamics, and that subsequent test programs could be launched based upon analysis of these findings. It was also envisioned that these data would be useful for calibrating computational fluid dynamics predictions of these aerodynamics. To help facilitate numerical analysis, the entire wing and near-field sting were developed as fully analytical surfaces, continuous through second derivative and, hence, curvature.

Facility and test conditions

The experimental program was performed in the National Transonic Facility. The NTF can be operated at Mach numbers ranging from 0.1 to 1.2, at total pressures from 1.1 to 8.8 atmospheres, and at total temperatures from around 120° F down to -250° F, the cryogenic temperatures being achieved through the evaporation of injected liquid nitrogen. The three degrees of freedom for controlling the test medium (speed, pressure, and temperature) allow for independent variation among the three primary aerodynamic freestream variables (Mach number, Reynolds number, and dynamic pressure). In the context of the present investigation, this capability can be exploited to eliminate certain pseudo-Reynolds number effects.[10] The facility test section is 8.2 feet square and approximately 25 feet long. Addition facility details can be found among Refs. 20-23.

The NTF operating envelope, scaled to the delta wing of the present investigation, is shown in Figure 1. Here the facility Reynolds numbers are based upon the delta wing mean aerodynamic chord and represent maximum operating capability. The Mach and Reynolds number extent for the delta wing experimental program is also shown and is well within the maximum facility capability. In addition, a variety of slender vehicle operating conditions are shown along with those for a typical High-Wing Military Transport (C-17). Although the delta wing is a very fundamental shape, the test program was designed to include conditions relevant to aircraft operations. A representative matrix of test conditions is shown in Figure 1b. Not all of these conditions were achieved for every configuration due to resource limitations.

Wind tunnel model

The model was a full-span delta wing mounted on an offset sting to obtain the desired angle of attack range. A photograph of the model along with some additional model details is provided in Figure 2. The off-set sting was designed to keep the model on the tunnel centerline for the full angle-of-attack range investigated.

The model was instrumented with 183 static surface orifices that had an internal diameter of 0.010 inches. (See Figure 2b.) The orifice arrangement allowed for fairly good spanwise resolution at five chordwise stations. Pressures were also located directly on the blunt leading edges to help track the onset and progression of leading-edge vortex separation. Pressures were measured remotely with electronically scanned pressure (ESP) modules.

The model was an uncambered flat plate with special consideration given to the leading and trailing edges. The wing was designed for a series of interchangeable leading-edge components and the leading edge contours are shown in Figure 3. They were defined with a NACA-like airfoil polynomial[24] for four values of leading-edge bluntness, r_{le}/c_{bar}, that were 0 (sharp), 0.0005, 0.0015, and 0.0030 in the streamwise direction. These bluntness values were chosen to be relevant to several aircraft that incorporate thin highly swept wings.[19]

The leading-edge contours matched the flat-plate wing over a distance of 15% root chord and were constant spanwise to match the flat-plate central

portion of the wing. This leading-edge contour region is also indicated in Figure 2b. The central flat plate portion of the wing was 5.1 percent thick (referenced to the mean aerodynamic chord) and this thickness was closed out over the last 10-percent of the root chord to a sharp trailing edge. The model was fabricated from VascoMax C-200, which is suitable for cryogenic testing. The model was polished to an 8-microinch surface finish.

Experimental procedures

Angle of attack was determined from the combination of arc-sector setting and calibrated sting-bending effects. Data were obtained at only two total temperatures, nominally 120^o F and -250^o F. Total pressure was varied nominally between 1.1 and 5.3 atmospheres to obtain the desired free stream test conditions.

No artificial transition strips were affixed to the model. It was anticipated that the flow would naturally be turbulent over the Reynolds numbers tested. Moreover, there were no clear transition-strip test techniques for these vortex flows.

A number of potential pseudo-Reynolds-number effects were considered and minimized in the design of the experiment. Calculations indicated that aeroelastic deformation would be small due to the low aspect ratio of the wing, the thickness of the wing, and the stiffness of the material. The 8-microinch surface finish was sufficient for the model to be hydraulically smooth over the range of conditions tested. Wind tunnel wall interference was believed to be negligible due to the slotted test section and the relative size of the delta wing to the test section (b/w_{ts} = 0.244). The model support mechanism was designed to keep the model centered in the test section. This essentially eliminated pseudo-angle-of-attack effects associated with the model traversing the test section flow and/or getting too close to the ceiling at high angles of attack.

RESULTS

Compressibility and Reynolds number effects for the sharp-edged delta wing are first presented. This is followed by an analysis contrasting the sharp and blunt-edged vortex flows at transonic speeds for a fixed angle of attack. An analysis contrasting low and high Reynolds number flows for the medium leading-edge bluntness is then presented, followed by discussion of the results for other leading-edge bluntness values. The initial analysis is focused at $\alpha = 11^o$ followed by angle-of-attack trends

Sharp-edge results

Compressibility. Although the emphasis of this paper is on transonic Reynolds number effects, some discussion of compressibility is warranted. Here we will simply contrast the vortex flows for a subsonic (M=0.4) and a transonic (M=0.85) condition.

Subsonic and transonic surface pressures are shown in Figure 4 for the sharp-edged delta wing at 11^o angle of attack and for a Reynolds number of 6 million. The subsonic results (M=0.4) show many features typical to sharp-edged delta-wing vortex flow. The primary vortex suction peak on the upper surface is evident at all pressure stations. It is located at approximately 80-percent semispan for most of the wing and also shows a longitudinal decrease in magnitude (i.e., less negative) from the wing apex to the trailing edge. Outboard of the primary suction peak the upper surface pressures are relatively constant in the spanwise direction which is typical for turbulent secondary vortex separation.

The transonic results (M=0.85) also show leading-edge vortex flow at all pressure stations. To illustrate some differences associated with this higher Mach number, a direct comparison of the subsonic and the transonic pressure for the 60-percent root-chord station is also shown in Figure 4. The data show two expected trends: at the transonic condition the suction peak has become less negative and has shifted inboard as compared to the subsonic results. The shift inboard is consistent with slender-wing theory.[3] The reduction in the primary vortex suction peak is consistent with transonic compressibility.

Further differences between the subsonic and transonic vortex flows can be appreciated from consideration of the sonic pressure coefficient, C_p^*. At M=0.4, $C_p^* = -3.7$ and the peak suction pressure at the 60-percent chord station is only about 38% of this value. The surface flow induced by the primary vortex is subsonic, not only at this station but for the entire wing. However, at M=0.85 $C_p^* = -0.3$, and virtually all the vortex induced pressures indicate supersonic flow.

Vacuum pressure considerations further contrast the subsonic and transonic vortex flows. At M=0.4, the vacuum pressure coefficient, $C_{p,v}$, is equal to -8.9, and the peak suction pressure coefficients are only a small percentage of this value. For example, at the 60-percent root-chord station, the peak suction pressure coefficient is 14% of $C_{p,v}$. However, at M=0.85 $C_{p,v}$ =-2.0, and the peak suction pressure coefficients are

significantly closer to this limiting value. As an example, the peak suction pressure coefficient at the 60-percent root-chord station is 59% of $C_{p,v}$. The characteristics of the transonic vortex flow are very different due to the supercritical flow induced by the leading-edge vortex.

Reynolds number. Transonic results are now presented at two Reynolds numbers for the sharp-edged wing at an angle of attack of 11°. See Figure 5. Although most comparisons for this paper will be made between Reynolds numbers of 6 million and 60 million, the highest Reynolds number tested for the sharp-edge configuration was 36 million.

The results presented in Figure 5 demonstrate that there is virtually no Reynolds number effect for the sharp edge wing at these conditions. These results are representative of other angles of attack as well, so for the sharp-edged wing there is very little Reynolds number effect at transonic speeds.

These results could be anticipated, since Reynolds number effects are known to be small for sharp-edged vortex flows. Hummel[2] has shown for subsonic speeds that a principal source of Reynolds number effects for the sharp-edged delta wing is the boundary layer state (laminar, transitional, or turbulent) for secondary vortex separation. These Reynolds number effects occur for longitudinal Reynolds number (based upon distance from the wing apex) less than a million, and can be important to experimental investigations at low speeds or with small models. However, at the Reynolds numbers for the present investigation these effects would be confined to a region very close to the wing apex and should be negligible.

Blunt-edge results

Bluntness. A comparison between the sharp and the medium-bluntness configurations is presented in Figure 6 at the low Reynolds number condition (6 million) and for a fixed angle of attack (11°). At the forward-most pressure station (20-percent root chord) the medium bluntness wing pressures indicate attached flow. At the 40-percent station the blunt-edge pressures look more like a leading-edge vortex signature, and by 60-percent root chord the pressures are clearly representative of vortex flow. These results demonstrate that, for the conditions shown, the blunt-edged wing has developed a part-span leading-edge vortex flow. The origin of this vortex is displaced from the wing apex, and from the results of Figure 6 it would be located somewhere between the 20-percent and the 40-percent root-chord stations. The detailed pressure comparison of Figure 6 shows that the blunt-edge pressures at the 60-percent root chord station are similar to the sharp-edge pressures for this Reynolds number.

Reynolds number. Whereas the sharp-edged vortex flow showed little Reynolds number effect, the blunt-edged flow exhibits significant effects of Reynolds number, especially as regards the onset and progression of leading-edge separation. An example is shown in Figure 7 for the medium leading-edge bluntness wing at Reynolds numbers of 6 million and 60 million. The surface pressures at the 40-percent root chord station exhibit attached-flow characteristics at the high Reynolds number; at the low Reynolds number these pressures indicated vortex flow. At the 60-percent station the pressures are directly contrasted in the inset of Figure 7, and the high Reynolds number data indicate neither a definitive attached-flow nor a definitive vortex-flow characteristic. This would imply the leading-edge vortex separation could have occurred slightly upstream of this station.

At the low Reynolds number, which is representative of conventional wind-tunnel conditions, this bluntness had a limited effect on the surface pressures. However, at the high Reynolds number, which is representative of flight conditions, this bluntness affected the pressures over the majority of the wing.

The Reynolds number effect on leading-edge separation is more clearly seen by contrasting the leading-edge pressure coefficients at the two conditions just discussed. The same surface pressure distributions from Figure 7 are repeated in Figure 8, but the inset pressure comparison is now for the leading-edge pressure coefficients, $C_{p,le}$. These coefficients are plotted against percent root chord, which is identical to fractional distance down the leading edge. The low and high Reynolds number data are identical down to 30-percent root chord, at which point the low-Reynolds number data indicate leading-edge separation. The high Reynolds number data indicate a further aft separation, perhaps near 50-percent root chord. By comparing the leading-edge pressure coefficients against the spanwise distributions in Figure 8, it is seen that they provide an indication of leading-edge separation. This same feature was shown[19] at M=0.4. The leading-edge pressure coefficients also demonstrate that the leading-edge flow is fully supersonic.

The leading-edge pressure coefficients are also indicative of the leading-edge suction. The low and

high Reynolds number data were integrated down the leading edge to estimate the aggregate effect of Reynolds number on leading-edge suction. The results indicate that the high Reynolds number flow developed 26% more leading-edge suction than the low Reynolds number case.

Thus far the analysis of Reynolds number effects has been focused at an angle of attack of 11^o. The Reynolds number effects are by no means restricted to this angle. In Figure 9 the leading-edge pressure coefficient at the 50-percent chord station is plotted as a function of angle of attack for the low and high Reynolds number conditions. The data show that the low and high Reynolds number results appear to be identical up to approximately 8^o angle of attack. Differences between the low and high Reynolds number data persist up to 18^o. The break in the low Reynolds number data at 8^o angle of attack (a local maxima) is an indication that the flow has separated. This effect is delayed by roughly 3^o for the high Reynolds number data.

This figure also shows the theoretical attached flow trend for the leading-edge pressure coefficients. The coefficients for this trend were obtained by performing a linear least-square fit to the high Reynolds number data at low angles of attack. The attached flow theory models the experimental trends very well up to an angle of attack of 6^o. Above this angle the data gradually depart from the theoretical trend before showing the reversal associated with leading-edge separation.

Thus far the data presented for the intermediate leading-edge bluntness has shown significant Reynolds number effects, not only over an extensive extent of the wing at a fixed angle of attack, but also over an extensive angle of attack range for a fixed leading-edge station. These effects are not restricted to this intermediate leading-edge bluntness.

Angle-of-attack trends for the leading-edge pressure at the 50-percent chord station are presented in Figure 10 for the three leading-edge bluntness values. In this figure the low and high Reynolds number data are compared for each of the leading-edge bluntness values. For the small leading-edge bluntness the Reynolds number effects are manifested for angles of attack ranging approximately from 4^o to 14^o. For the large leading-edge bluntness the Reynolds number effects begin around 10^o and persist over the range of data obtained. Thus, these data demonstrate that an increase in leading-edge bluntness delays the manifestation of the subject Reynolds number effects to higher angles of attack.

These same data are cross-plotted in Figure 11 to show the effect of leading-edge bluntness at low and high Reynolds number. At the low Reynolds number leading-edge bluntness ceases to have an effect on the data above 15^o angle of attack. At the high Reynolds number leading-edge bluntness affects the data over the range of angles of attack tested. Similar results to Figures 10 and 11 were found at the 30-percent (Figure 12) and 70-percent (Figure 13) root-chord stations.

FINAL REMARKS

An analysis of Reynolds number and leading-edge bluntness effects for the flow about a 65^o delta wing has been presented. Analysis was focused upon data obtained at a free stream Mach number of 0.85 out of an extensive data set generated in the NTF.

A limited analysis of data for the sharp-edged delta wing demonstrated that there are negligible Reynolds number effects for this configuration. Compressibility analysis also showed that for the transonic condition the flow induced by the leading-edge vortex is locally supersonic over much of the wing upper surface.

The supersonic flow was sustained for the blunt leading-edge configurations analyzed, and the flow down the blunt leading edge itself was also shown to be supersonic. However, significant Reynolds number effects were also demonstrated for all three values of leading-edge bluntness. These differences were primarily associated with Reynolds number effects on the onset and progression of leading-edge vortex separation. They were manifested over a significant fraction of the wing upper surface (at a fixed angle of attack) as well as over an extensive angle of attack range (at a fixed location).

Although the analysis was limited to comparisons of low (6 million) and high (60 million) Reynolds number data, these differences are significant since these two Reynolds number values are comparable to typical ground-based wind tunnel conditions and flight conditions, respectively. Additional analysis of this data set for Reynolds number trends could provide scaling guidance for ground-based testing of these flows.

REFERENCES

[1]Polhamus, E. C., "A Concept of the Vortex Lift of Sharp-Edged Delta Wings Based on a Leading-Edge Suction Analogy," NASA TN D-3767, 1966.

[2]Hummel, D., "On the Vortex Formation Over a Slender Wing at Large Incidence," AGARD CP-247, Paper No. 15, January 1979.

[3]Smith, J. H. B., "Improved Calculations of Leading-Edge Separation from Slender Delta Wings". RAE TR-66070, 1966.

[4]Hemsch, M. J., and Luckring, J. M., "Connection Between Leading-Edge Sweep, Vortex Lift, and Vortex Strength for Delta Wings," AIAA J. Aircraft, Vol. 27, No. 5, May 1990.

[5]"High Angle of Attack Aerodynamics," AGARD CP-247, January 1979.

[6]"Aerodynamics of Vortical Type Flows in Three Dimensions," AGARD CP-342, July 1983.

[7]"Vortex Flow Aerodynamics," AGARD CP-494, July 1991.

[8]Lynch, F. T., "Commercial Transports – Aerodynamic Design for Cruise Performance Efficiency," Transonic Aerodynamics, Progress in Astronautics and Aeronautics, Vol. 81, 1982.

[9]Goldhammer, M. E., and Steinle, F. W., Jr., "Design and Validation of Advanced Transonic Wings Using CFD and Very High Reynolds Number Wind Tunnel Testing," 17th ICAS Congress, September 1990.

[10]Elsenaar, A., Binion, T. W. Jr., and Stanewsky, E., "Reynolds Number Effects in Transonic Flow," AGARDograph AG-303, December 1988.

[11]Haines, A. B., "Scale Effects on Aircraft and Weapon Aerodynamics," AGARDograph AG-323, July, 1994.

[12]Henderson, W. P., "Study of Various Factors Affecting Drag Due to Lift at Subsonic Speeds," NASA TN D-3584, October 1966.

[13]Polhamus, E. C., "A Survey of Reynolds Number and Wing Geometry Effects on Lift Characteristics in the Low Speed Stall Region," NASA CR-4775, June 1996.

[14]Polhamus, E. C., "A Review of Some Reynolds Effects Related to Bodies at High Angles of Attack," NASA CR-3809, August 1984.

[15]Chu, J., and Luckring, J. M., "Experimental Surface Pressure Data Obtained on 65° Delta Wing Across Reynolds Number and Mach Number Ranges. Volume 1 – Sharp Leading Edge," NASA TM-4645, February 1996.

[16]Chu, J., and Luckring, J. M., "Experimental Surface Pressure Data Obtained on 65° Delta Wing Across Reynolds Number and Mach Number Ranges. Volume 2 – Small Leading Edge," NASA TM-4645, February 1996.

[17]Chu, J., and Luckring, J. M., "Experimental Surface Pressure Data Obtained on 65° Delta Wing Across Reynolds Number and Mach Number Ranges. Volume 3 – Medium Leading Edge," NASA TM-4645, February 1996.

[18]Chu, J., and Luckring, J. M., "Experimental Surface Pressure Data Obtained on 65° Delta Wing Across Reynolds Number and Mach Number Ranges. Volume 4 – Large Leading Edge," NASA TM-4645, February 1996.

[19]Luckring, J. M., "Reynolds Number and Leading-Edge Bluntness Effects on a 65° Delta Wing," AIAA Paper 2002-0419, January 2002.

[20]Wahls, R. A., "The National Transonic Facility – A Research Retrospective," AIAA Paper 01-0754, January 2001.

[21]Luckring, J. M., "An Overview of National Transonic Facility Investigations for High Performance Military Aerodynamics" AIAA Paper 01-0906, January 2001.

[22]Fuller, D. E., "Guide for Users of the National Transonic Facility," NASA TM-83124, 1981.

[23]Foster, J. M., and Adcock, J. B., "Users Guide for the National Transonic Facility Research Data System," NASA TM-110242, April 1996.

[24]Abbott, I. H., and Von Doenhoff, A. E. "Theory of Wing Sections," Dover Publications, Inc., 1959.

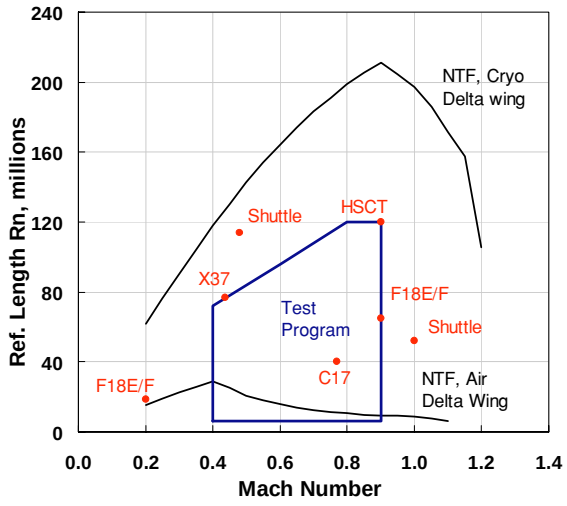

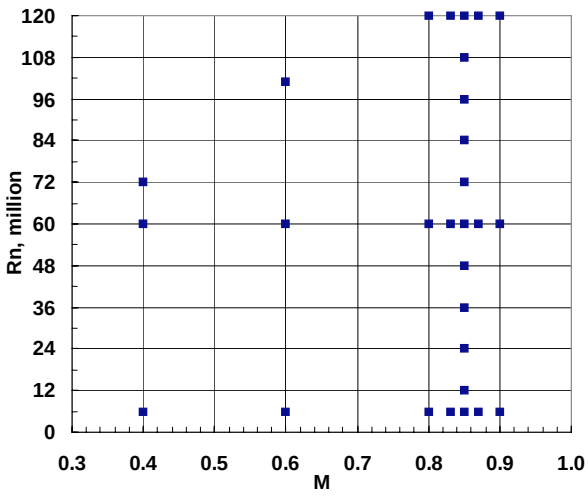

a) NTF envelopes and aircraft operating conditions.

b) Representative delta-wing test matrix.

Figure 1 – Reynolds number and Mach number conditions.

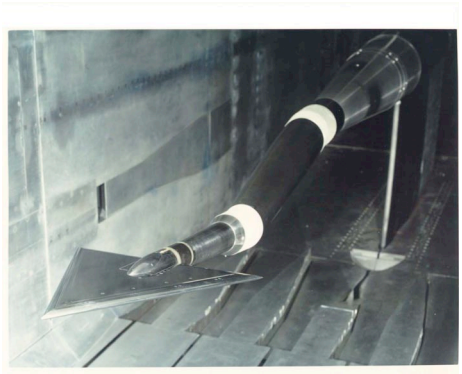

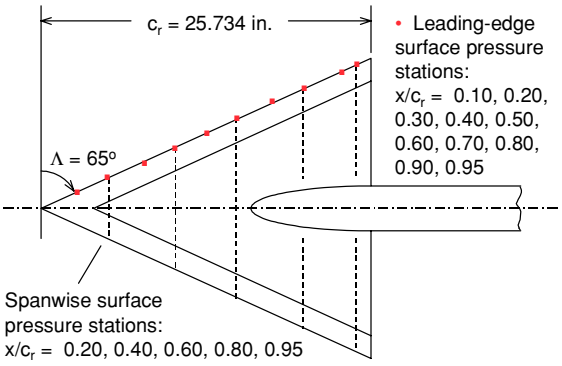

a) Model installed in NTF.

b) Instrumentation layout.

Figure 2 – NTF 65° delta wing.

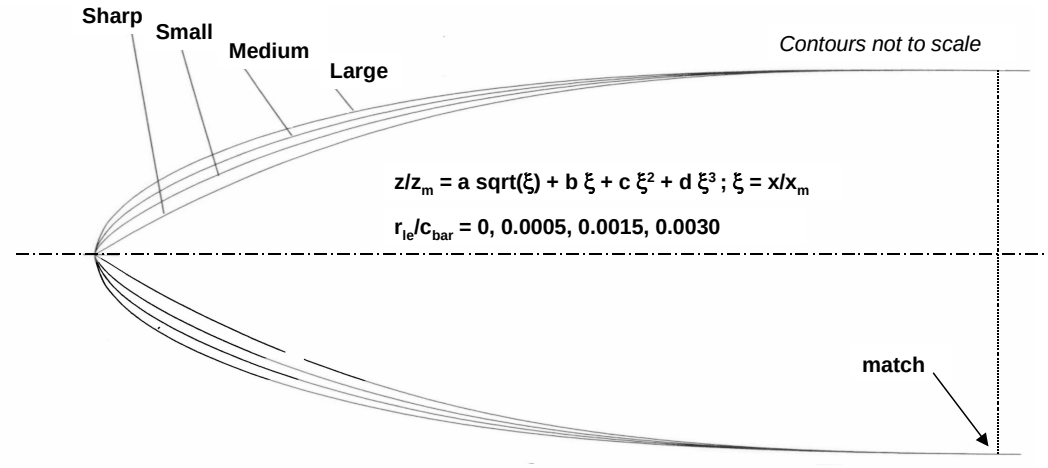

Figure 3 – Streamwise leading-edge contours for NTF delta wing.

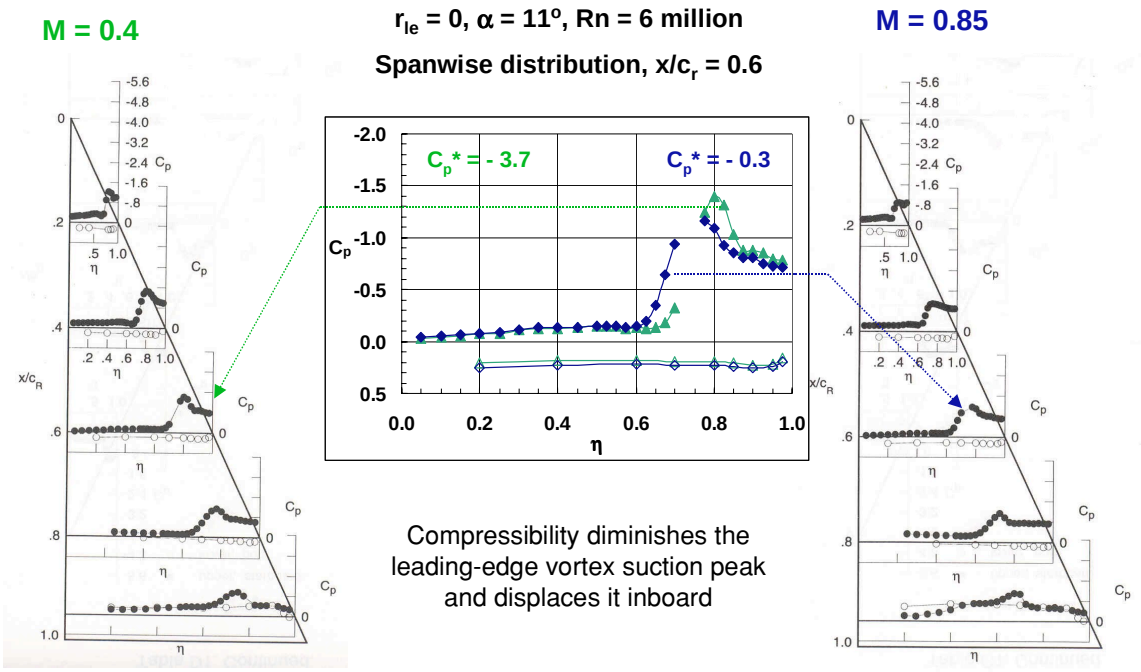

Figure 4 – Compressibility effect on sharp-edged vortex flow.

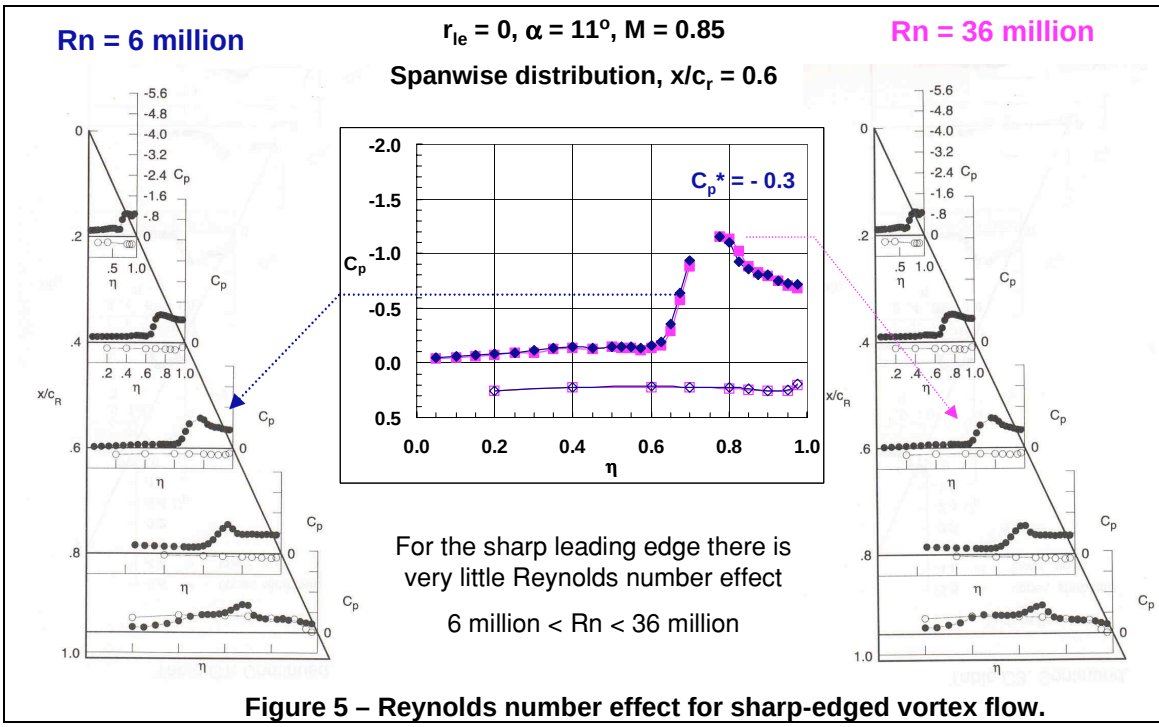

Figure 5 – Reynolds number effect for sharp-edged vortex flow.

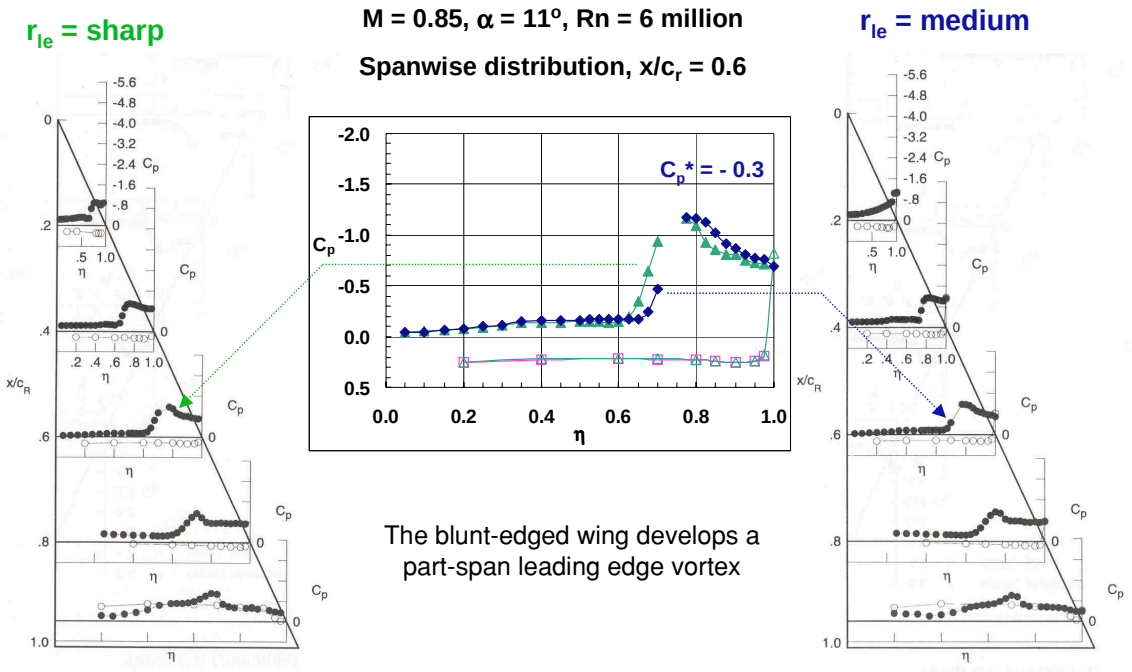

Figure 6 – Bluntness effect at low Reynolds number.

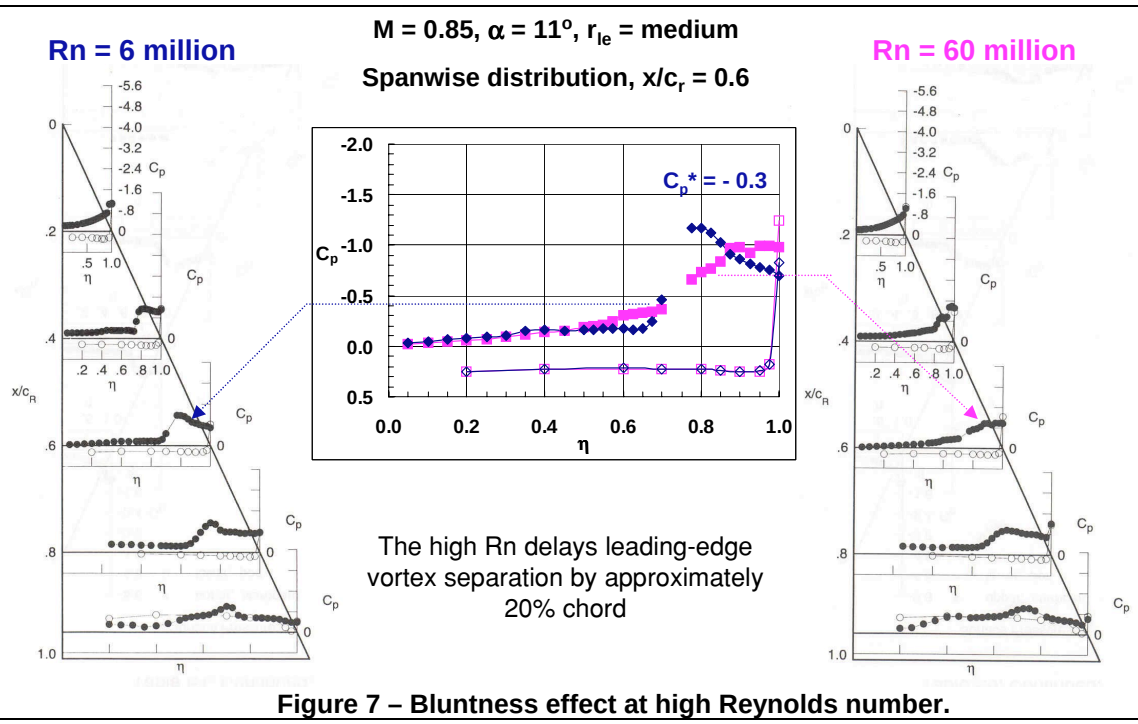

Figure 7 – Bluntness effect at high Reynolds number.

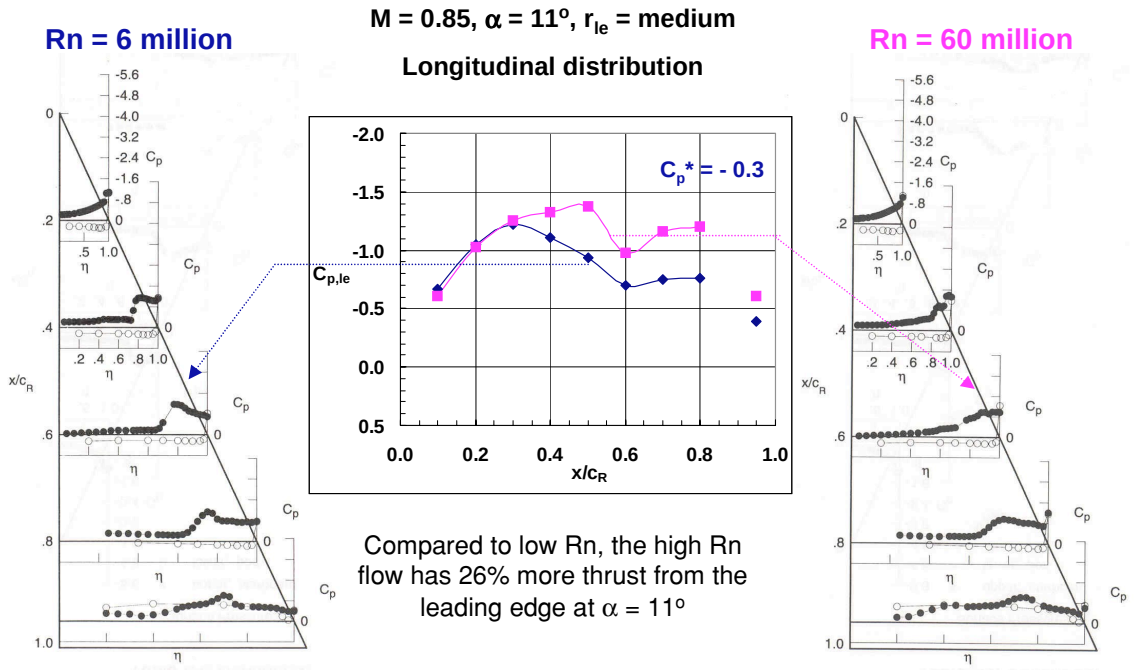

Figure 8 – Longitudinal distribution of leading-edge Reynolds number effect.

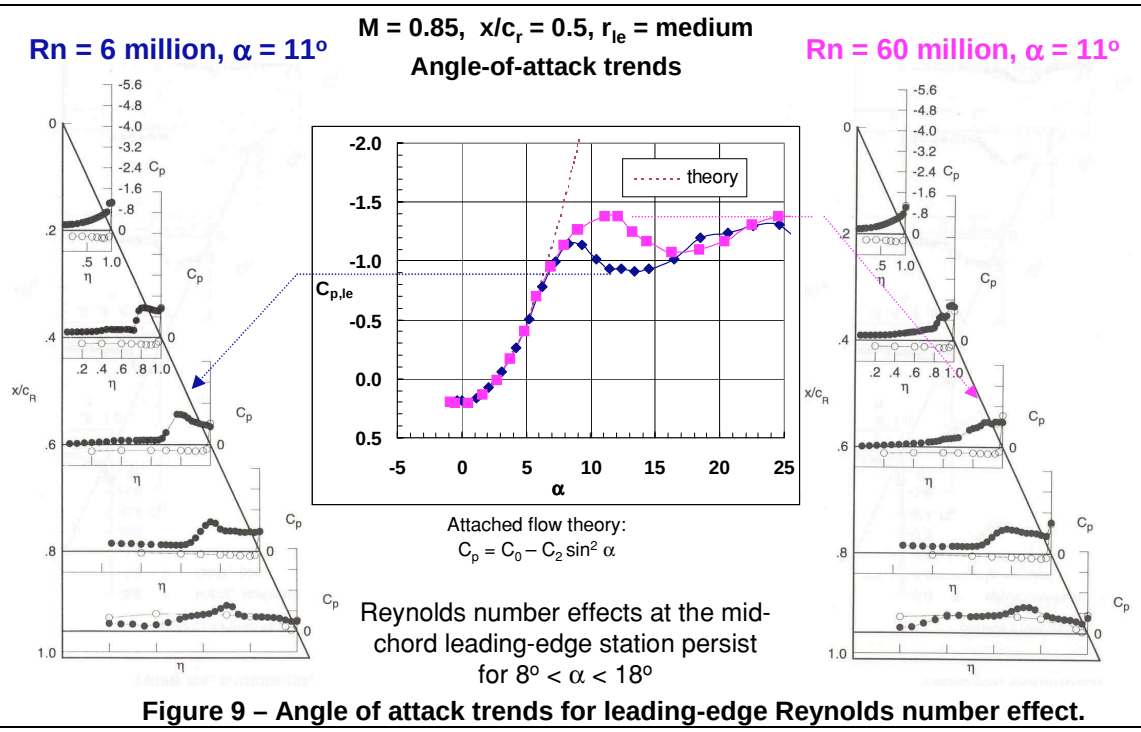

Figure 9 – Angle of attack trends for leading-edge Reynolds number effect.

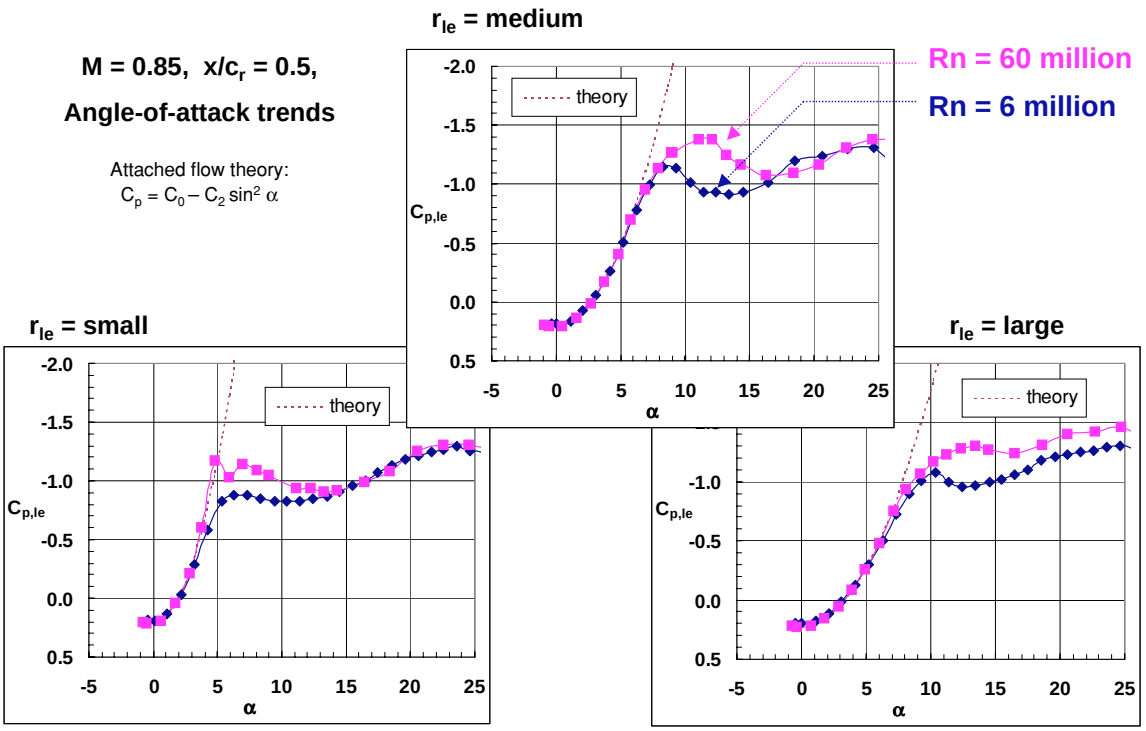

Figure 10 – Reynolds number effects for 3 leading-edge bluntnesses.

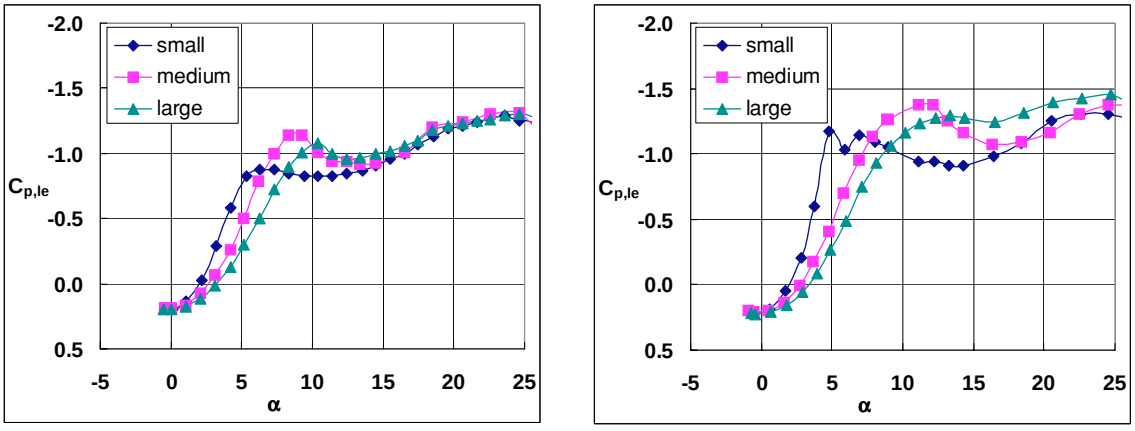

Figure 11 – Leading-edge bluntness effects at low and high Reynolds numbers. x/c_r=0.5.

M = 0.85, x/c_r = 0.3,

Angle-of-attack trends

Rn = 6 million

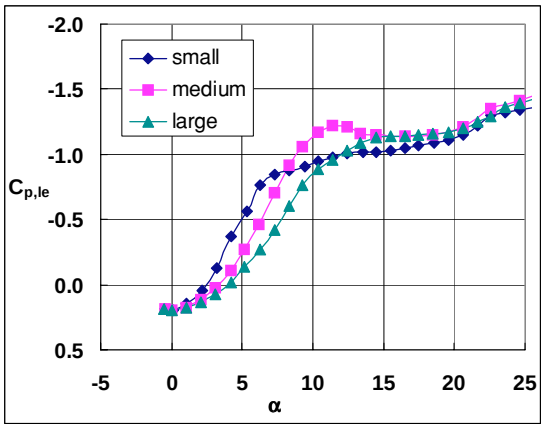

Rn = 60 million

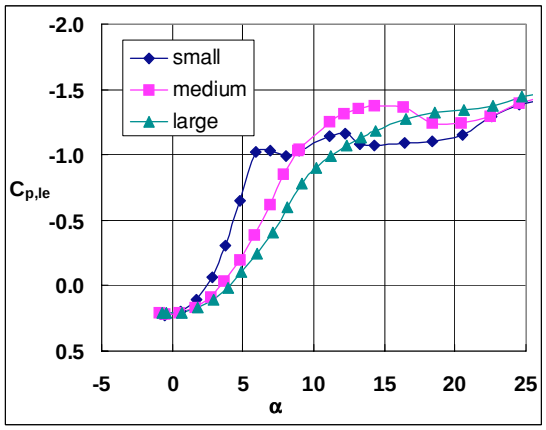

Figure 12 – Leading-edge bluntness effects at low and high Reynolds numbers. x/c_r=0.3.

M = 0.85, x/c_r = 0.7,

Angle-of-attack trends

Rn = 6 million

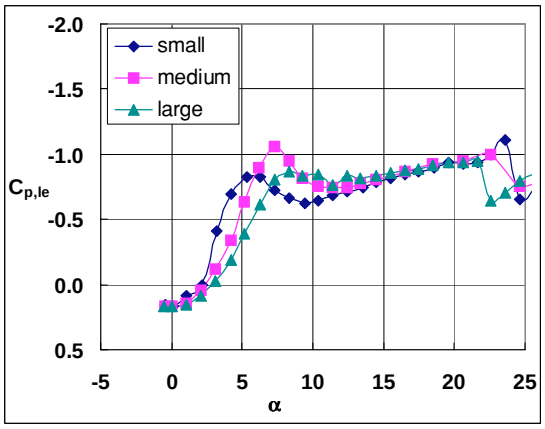

Rn = 60 million

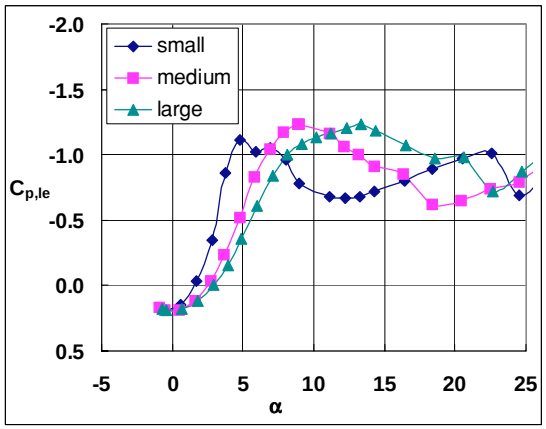

Figure 13 – Leading-edge bluntness effects at low and high Reynolds numbers. x/c_r=0.7.